# Determining the Vignetting and Echelle Blaze Function for the GHRS

R. D. Robinson[1]

**Abstract**

I describe the techniques used in deriving the vignetting in the GHRS when used with the first order gratings G140M, G160M, G200M, G270M and G140L. I also present an analysis of the blaze function and vignetting present in the echelle B data.

## I. Introduction

The sensitivity function of the spectrograph is simply a conversion factor between count rate and absolute flux at any given wavelength. Inspection of the data immediately reveals, however, that the value of the sensitivity can be highly dependent on the position of that wavelength sample on the photocathode of the detector. For the first order gratings the sensitivity is a three dimensional function of the variables X, Y and λ. For the echelle gratings we have the additional complication of the blaze or ripple function, where for any given order the response peaks at a given wavelength and decreases at both higher and lower wavelengths.

To simplify the problem we have separated the total spectrograph sensitivity into a variety of components. The simplest and most easily calculated is the standard sensitivity, defined for first order gratings as the conversion between count rate and absolute flux at the center of the detector. For the echelle the sensitivity is the conversion factor measured at the peak of the blaze function for each order. Large scale variations in this sensitivity along both the X and Y directions are then identified as vignetting, which includes the influence of obstructions within the light path as well as such effects as losing light from the wing of the PSF off the end of a diode, non-uniformities in the photocathode faceplate (sleeks) and large scale variations in the gain of the diodes or the response of the photocathode. Small scale imperfections on the photocathode are referred to as blemishes and are discussed by Wahlgren, et al (this volume), while small scale, small amplitude (1-2 percent) gain variations from the photocathode or diodes are referred to as granularity and discussed by Cardelli (this volume).

In this paper we describe the procedures used to determine the vignetting and blaze functions for the GHRS gratings as well as the results themselves. The reduction procedures are described so that the general user can understand the limitations of the final calibrations.

---

1. CSC, Goddard Space Flight Center, Code 681/CSC, Greenbelt, MD 20771

## II. Vignetting in the First Order Gratings

The data used in deriving the vignetting were taken during the science verification (SV) phase of the mission. Observations of μ Columbae were used to calibrate all of the medium resolution gratings (G140M, G160M, G200M and G270M). Observations of this star were supplemented by observations of the fainter BD+25D325 in calibrating the low resolution (G140L) grating. The data consisted of sequences of exposures taken over the entire useful wavelength range of each first order grating and with an approximately 50 percent overlap in wavelength coverage between adjacent exposures. Thus, nearly all wavelengths were sampled at two positions on the detector. In figure 1 we show an overlapping plot of some of the G270M data illustrating the effects of vignetting on the data.

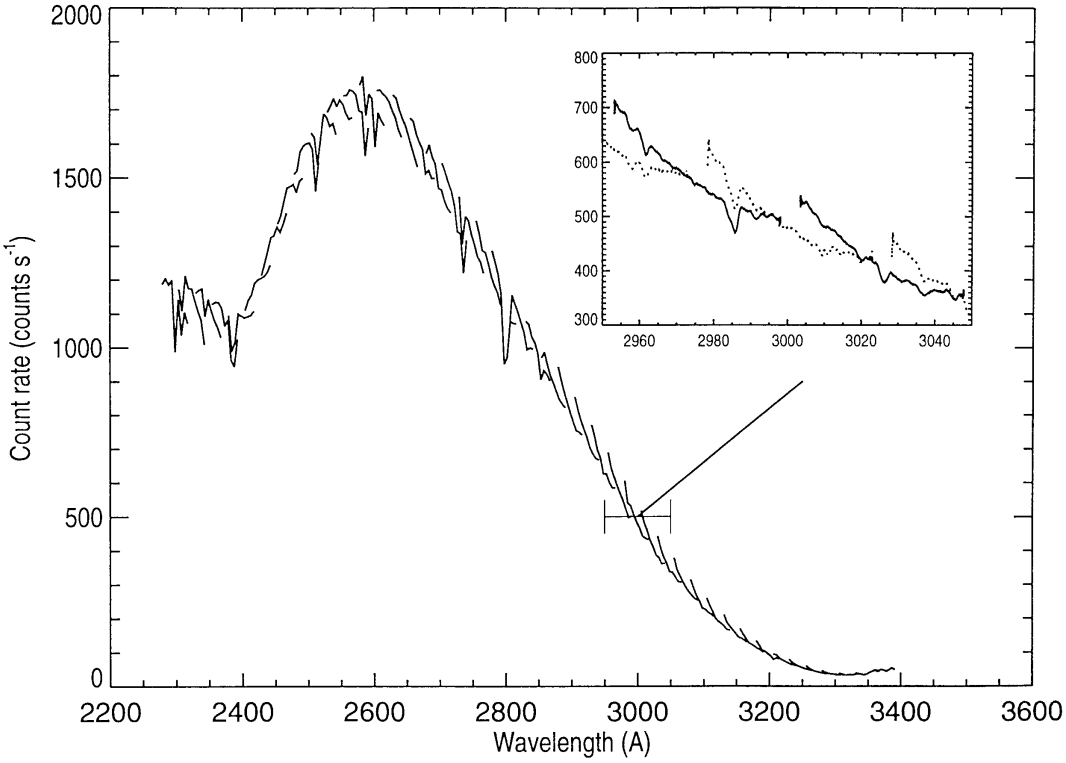


Figure 1: Overplot of the G270M calibration data showing the effects of vignetting. The large scale trends are caused by sensitivity variations.

The basic technique for measuring the vignetting was to use a simple sensitivity calibration to calculate the absolute flux for the data and then compare the calculated flux with that from a reference spectrum. The large scale differences between the two were then attributed to vignetting. The diode array spans nearly the full width (x-dimension) of the photocathode. Since the spectrum is slightly tilted with respect to the x-axis, changing the wavelengths of the observation moved the observations along the y dimension. Thus, by analyzing spectra taken at different wavelengths you can build up a complete two dimensional picture of the vignetting function.

In practice the analysis is somewhat more complicated. Firstly, the original reference spectrum for μ Columbae was taken with the IUE in low resolution mode and had

very low spectral resolution, typically about 5Å compared with resolutions of 0.57Å for the G140L and 0.05-0.1Å for the medium resolution gratings. This IUE spectrum worked reasonably well for the G140L data and for the medium resolution gratings at wavelengths greater than 1900Å. It was totally inadequate, however, for analyzing the medium resolution observations at shorter wavelengths, where substantially more fine structure is present. For these wavelengths we first determined a vignetting function for the G140L grating using the IUE spectrum, applied these vignetting corrections to the G140L data and then merged the individual spectra into a low resolution GHRS reference spectrum covering the wavelength range between 1100Å and 1900Å. This spectrum was then used as a reference in analyzing the medium resolution observations.

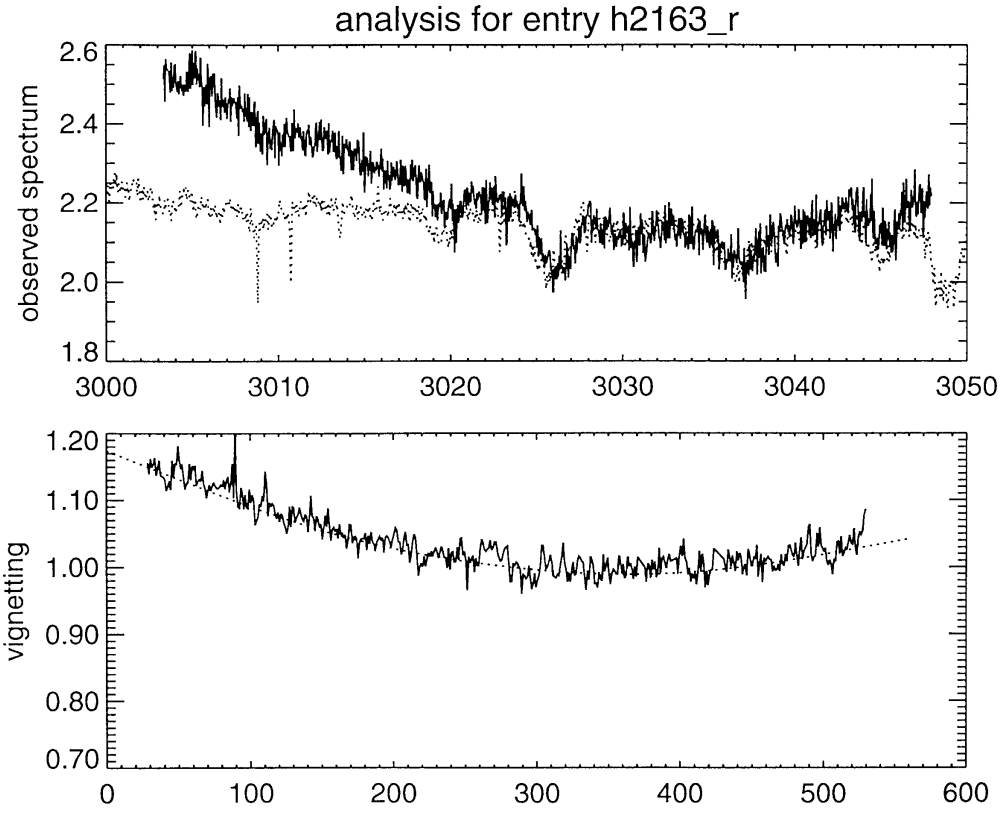


Figure 2: Analysis of the vignetting in a single exposure taken with the G270M grating. The low resolution *IUE* reference spectrum is shown as a dotted line in the top plot.

Figure 2 shows an example of the vignetting calculation for an individual spectrum. In many cases it was necessary to reduce the resolution of the observations to that of the comparison spectrum by convolving with an appropriate instrumental profile. A cross correlation was also performed and the calibration spectrum was shifted to align as closely as possible with the data. The raw vignetting curve normally had a substantial fine structure which is caused by noise, calibration errors in the comparison spectrum, inaccuracies in degrading the resolution of the observation, as well as blemishes on the photocathode. While some of this structure may be real we found that it was better to deal with it as blemishes rather than vignetting and eliminated it from the final vignetting curve by fitting a smooth, low-order spline to the data. Typically, 5 nodes were found to give an acceptable fit.

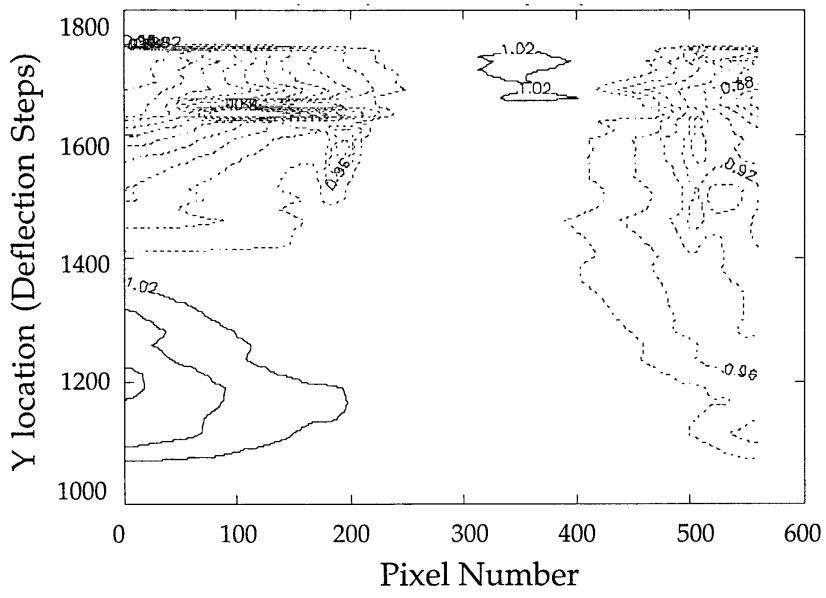


Figure 3: A total vignetting function for the G140M grating, done before smoothing in the Y direction. Note the large "scratch" near Y location 1625. Details of the plot are given in Figure 5.

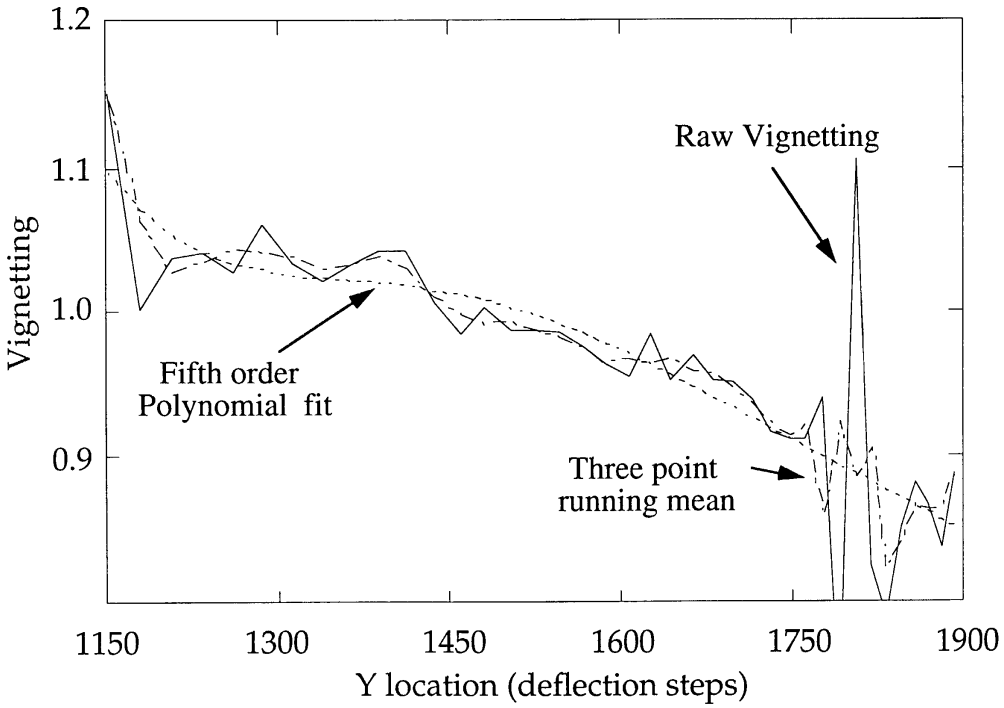


Figure 4: Smoothing the vignetting function in the Y direction. A 3 point running mean was found to give the best results.

The vignetting curves for the individual wavelength settings were eventually merged into an image, which represented the full vignetting function for that particular grating. Figure 3 shows a sample, raw vignetting function for grating G1. The noise is caused by errors in the spline fits to the individual vignetting curves as well as the fact that the vignetting may change dramatically over the 400 μm height of an individual diode. Note, for example, the very sharp feature at the Y location of 1650 deflection units, which is caused by a sizable scratch in the photocathode.

Figure 4 shows a slice of the image along the Y direction (e.g. at constant sample position) and illustrates the large scale trends which we want to retain. Several schemes were tried for smoothing the data along the Y direction, including polynomial and spline fits. In the end it was decided that a simple three point running mean was sufficient to smooth the data without overly distorting the large scale trends. The final, smoothed vignetting functions are presented in figure 5.

## III. Calibrating the Echelle Data

*The Echelle B Blaze Function*

A well known characteristic of echelle spectrographs is that the sensitivity for a specific order peaks at a given wavelength and decreases at both higher and lower wavelengths. This is the so-called blaze function and has approximately a constant shape when plotted against the variable $m\lambda$, where m is the order number and $\lambda$ is the wavelength. There were extensive pre-launch tests of the echelle characteristics, and it was thought that in-orbit calibrations only needed to sample the full calibration. These data would then allow us to adjust the groundbased calibrations and thereby obtain the full on-orbit characteristics. As shown below, this strategy turned out to be only marginally successful.

The star μ Columbae was again chosen as the spectrophotometric standard. The pattern of exposures taken during SV tests designed to study sensitivity, vignetting and ripple for the echelle B grating are shown schematically in figure 6. SV tests designed to measure the echelle A grating characteristics failed during execution and the side 1 electronics failed before these tests could be rerun. The blaze function tests consisted of sequences of exposures at different wavelengths along an individual order (termed a WSCAN) covering the entire useful wavelength range for 6 of the 16 orders. Sensitivity and vignetting were to be calculated using scans of all of the orders (termed an OSCAN) at 3 specific values of $m\lambda$, one near the peak of the response function and one at each end of the free spectral range.

The analysis began by determining the basic sensitivity function, which was defined as the conversion between count rate and absolute flux as measured at the peak of the blaze function for each order. These calculations were carried out using the central OSCAN. This sensitivity function was then used to determine a rough absolute flux calibration for each spectrum in the WSCAN taken over individual orders. The results of such a calculation are shown in figure 7, which clearly shows the effects of both the vignetting and the blaze function. The roughly calibrated data go to higher fluxes than the reference because the sensitivity was not measured exactly at the blaze maximum.

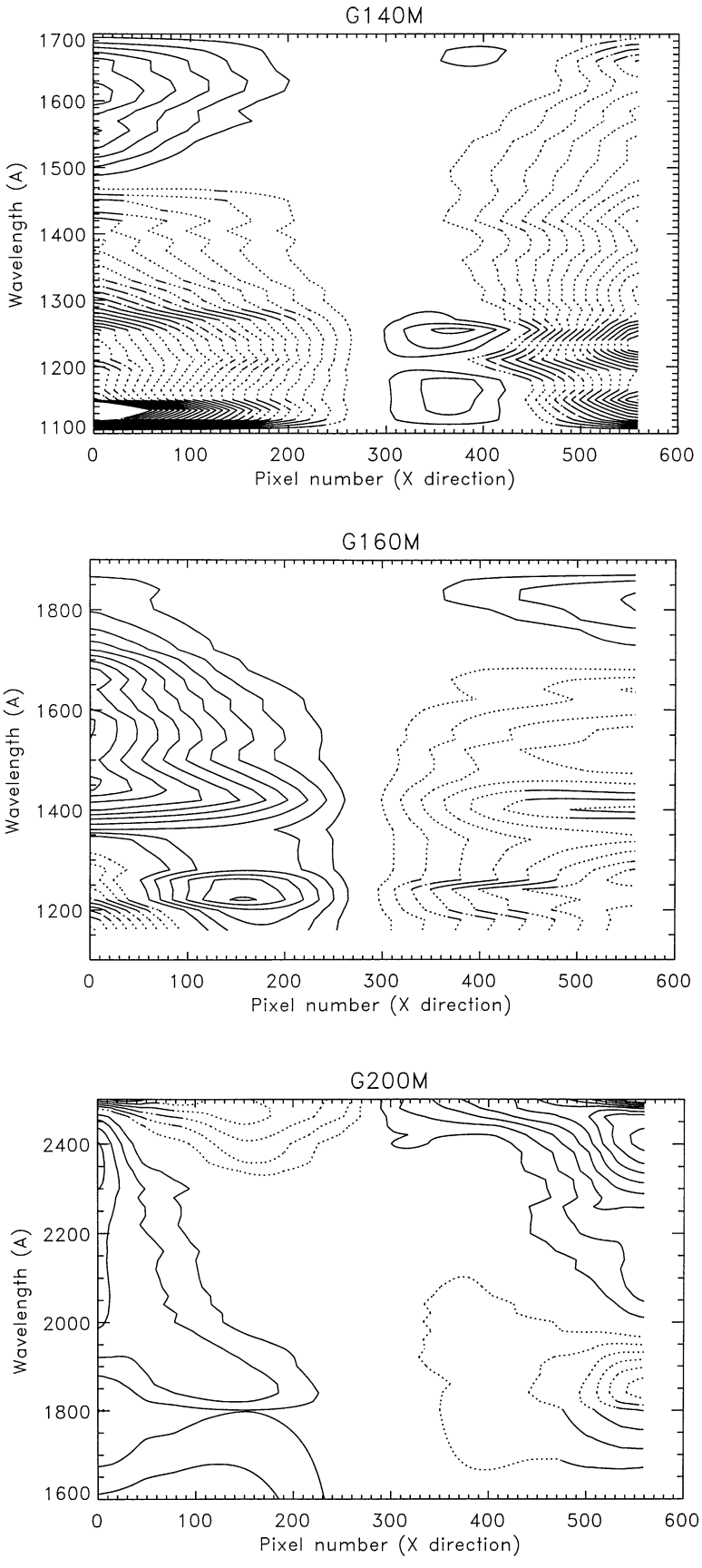
G140M
Wavelength (A)
1700
1600
1500
1400
1300
1200
1100
0
100
200
300
400
500
600
Pixel number (X direction)
G160M
Wavelength (A)
1800
1600
1400
1200
0
100
200
300
400
500
600
Pixel number (X direction)
G200M
Wavelength (A)
2400
2200
2000
1800
1600
0
100
200
300
400
500
600
Pixel number (X direction)

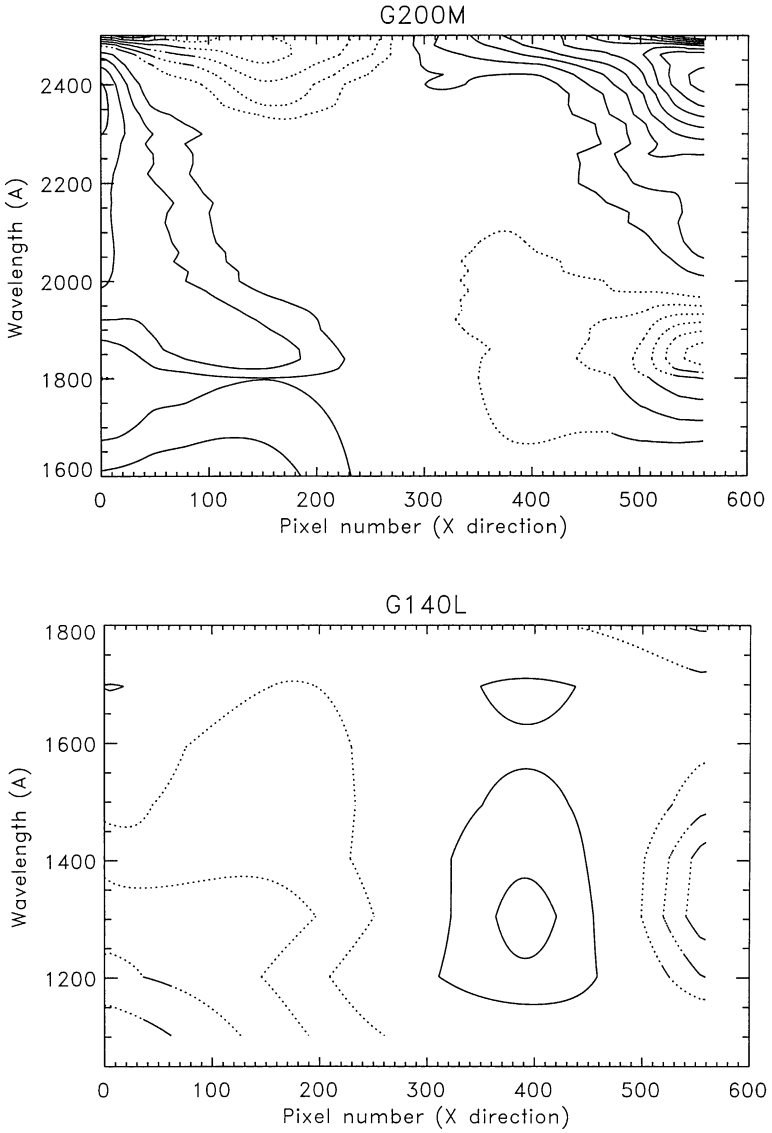


Figure 5: Final vignetting for the first order gratings. These are correction factors for the data, defined to be 1 at the center of the diode array. The spacing is in intervals of 1 percent, with the solid lines being greater than unity (e.g. 1.01, 1.02, etc.), while the dotted lines are less than unity (e.g. 0.99, 0.98, etc). The corrections are made by dividing the observed counts by the vignetting.

To calculate the blaze function ($R$), the absolute flux from the *center* of each of the spectra in the WSCAN was compared with the flux in a reference spectrum, derived by combining the calibrated, vignetting corrected spectra obtained during the first order gratings tests. A non-linear least squares fit was then determined between the measured corrections and a theoretical curve based on equation 18 in Bottema (1980, SPIE Proc, 240, 171);

$$R = C \times N \times \mathrm{sinc}^2(X) ,$$

where,

$$N = \cos(\theta + \beta + \delta) / \cos(\theta + \beta - \delta),$$
$$X = \pi \times m \times \cos(\theta + \beta + \delta) \times \sin(\theta) / \sin(\theta + \beta), \text{ and}$$
$$\theta = (R0 - CP) / 182.0444 - \beta$$

Here $\beta$ is the echelle blaze angle, $\delta$ is the half angle between the collimator and the cross disperser, $\theta$ is the grating angle, *R0* is the reference carrousel position specifying the point of maximum sensitivity, *C* is a normalization constant, *CP* is the carrousel position and *m* is the order number. In the fitting process values of $\beta$, $\delta$, *R0* and *C* were determined for each order. Ideally, these should be identical for all orders, since they refer to physical properties of the spectrograph. In practice their values varied between orders, giving the curves shown in figure 8. This behavior was expected, since it occurred in the ground-based tests (see the pre-launch calibration report for the GHRS).

Rather than use separate values of $\beta$, $\delta$ and *R0* for each order, it was decided to adopt representative values and introduce 'fudge factors' into the expression to account for deviations from the norm. To do this we replace the variable *X* with *X'*, such that;

$$X' = A \times X + B$$

where *A* and *B* are the fudge factors, with *A* controlling the width of the function and *B* determining the position of the sensitivity maximum. Unfortunately, the representative values for $\beta$, $\delta$, and *R0* determined from the on-orbit calibrations differed significantly from the values obtained from the ground, so that none of the results of the ground-based calibrations could be used in the on-orbit calibration.

In figure 9 we show the best fit of the theoretical blaze function to the observations in order 20, using single values for *A* and *B*. The results give extremely good agreement with the observations. Unfortunately, this fitting could only be done for those orders for which a full WSCAN was available. To determine the fudge factors in the other orders we did a linear least-squares fit to the best single values of *A* and *B* for the WSCAN orders, as shown in figure 10. Note that while the values of *B* give a reasonably well defined, linear trend with order number, the values of *A* have considerably more scatter.

*Vignetting in Echelle B*

Figure 11 shows an overlap of the spectra taken in the order 20 WSCAN after conversion to absolute flux and correction for the echelle blaze function. A significant vignetting is obviously present. The vignetting also changes significantly with wavelength, even though the range of Y positions of the photocathode which is sampled by this data is small. To determine a representative vignetting function for the echelle we used the same OSCAN data which was used to derive the absolute sensitivity curve. This sampled all of the orders near the center of the free spectral

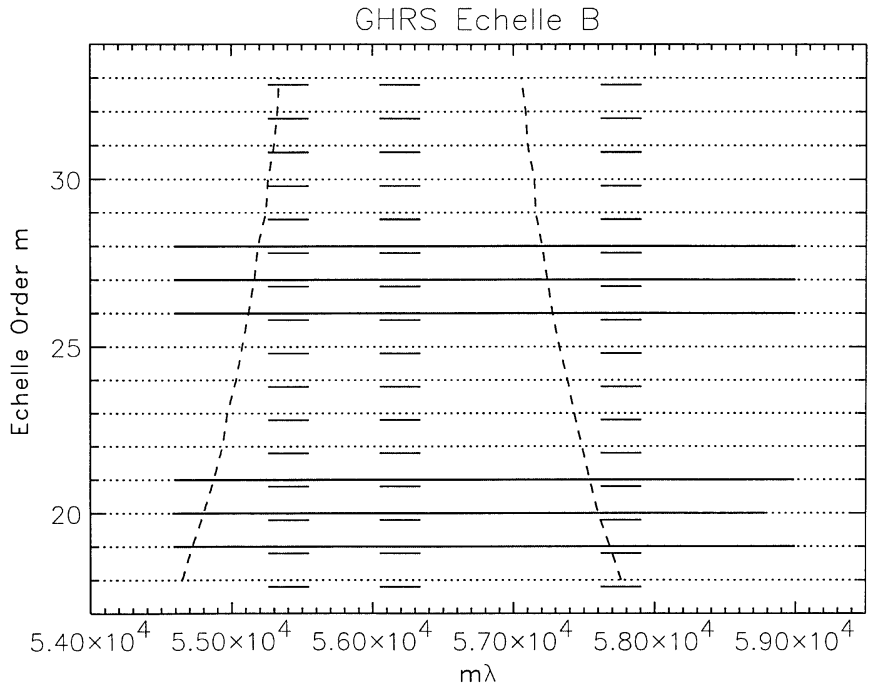


Figure 6: Wavelength and orders observed during the SV tests designed to measure echelle sensitivity, vignetting and blaze function.

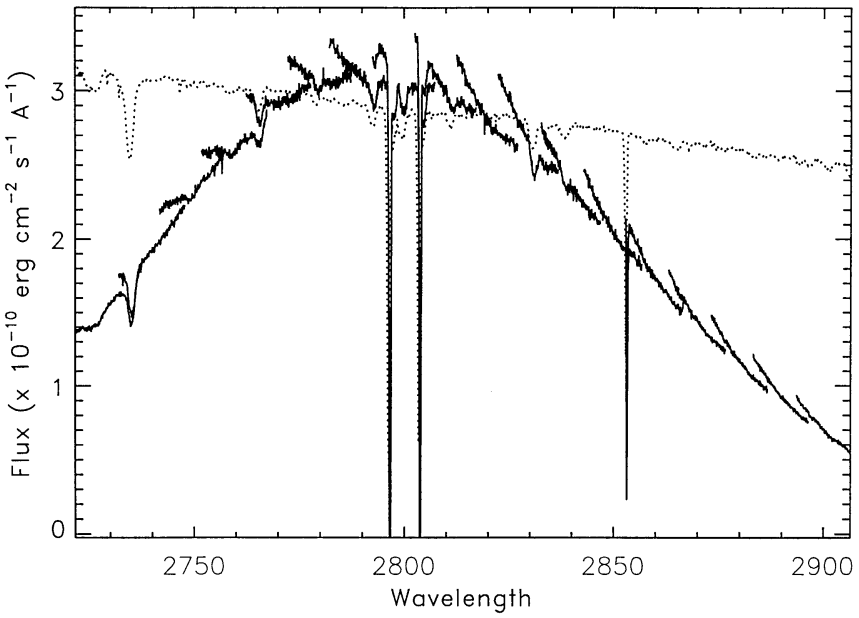


Figure 7: Overplot of the WSAN data for order 20 (solid). The reference spectrum, which shows the correct flux levels, is given by the dotted line.

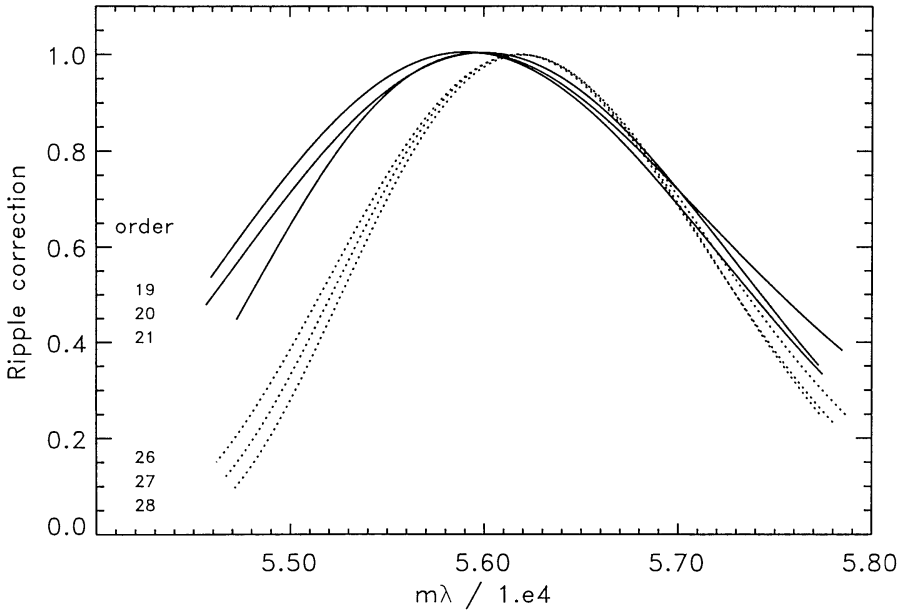


Figure 8: Measured blaze function for the 6 orders with good wavelength coverage.

.

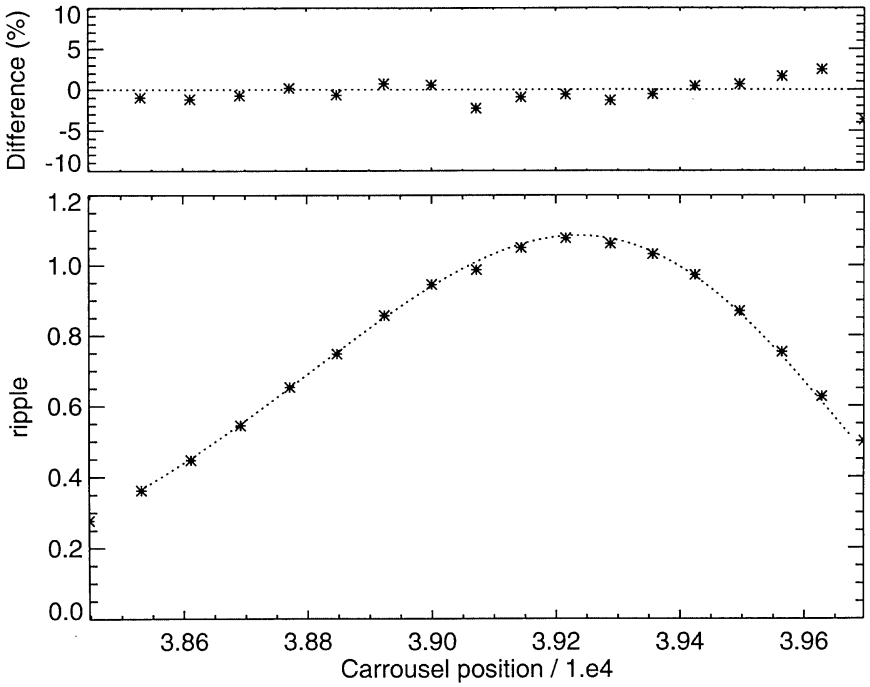


Figure 9: Results of the fitting of the observations to the theoretical formalism described in the text.

range and covered nearly the entire surface of the photocathode. The method of analysis was nearly identical to that used in determining vignetting for the first order gratings, except that the reference spectrum was the medium resolution GHRS atlas of μ Col which was generated from data obtained for the first order grating calibrations.

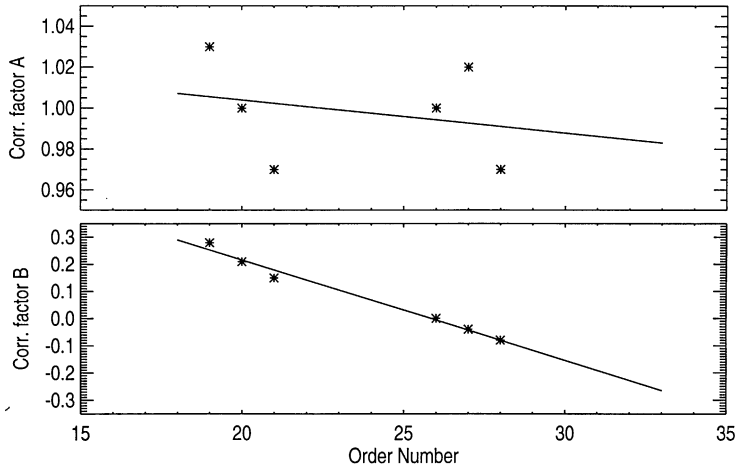


Figure 10: Fudge factors A and B for the 6 orders with good wavelength coverage. The lines show the least squares fit to the data and were used to determine the blaze functions for other orders.

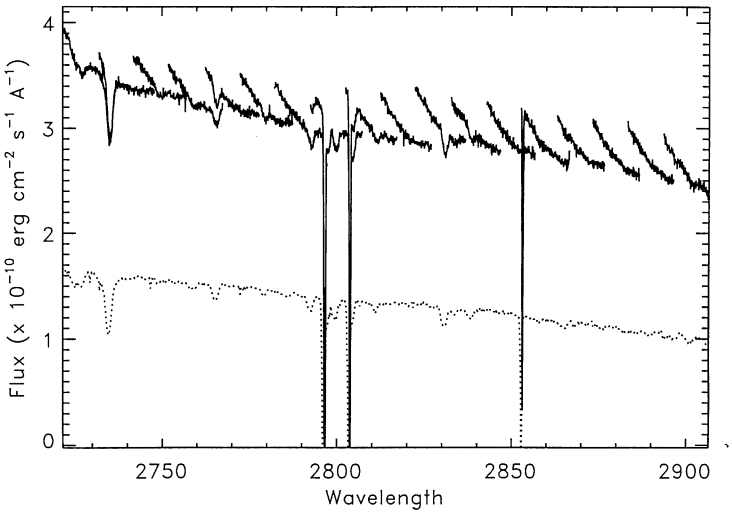


Figure 11: Overplot of the WSCAN data from order 20 after correcting for the blaze function. The reference spectrum, shown as a dotted line, has been displaced downward.

The results of the analysis are shown in figure 12. Repeating the analysis for the OSCANS taken at the high and low wavelength limits of each order produced vignetting functions which differed from the function presented in figure 12 by factors of up to 20 percent.

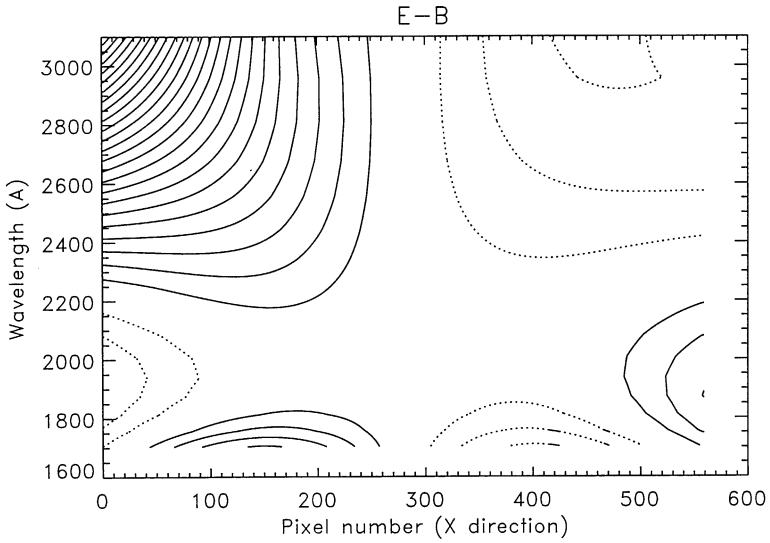


Figure 12: The vignetting function for echelle B as derived from data obtained from the central OSCAN. Details of the curves are as presented in Figure 5.

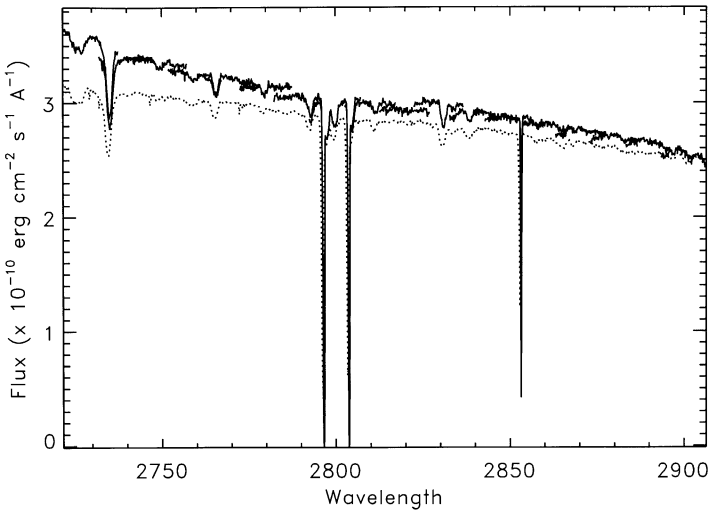


Figure 13: Overplot of the WSCAN data for order 20 after correcting for both the blaze function and vignetting. The reference spectrum (dotted) has been displaced downward slightly.

## Conclusions

Overall, the total, multi-dimensional sensitivity characteristics of the GHRS gratings are reasonably well understood and relative fluxes which are good to about 5 percent should be attainable on a regular basis. One of the primary existing problems with first order vignetting involves corrections near the ends of the array (i.e. near the edge of the photocathode), where the existing functions sometimes overcorrect or

undercorrect by as much as 10 percent. This is not always seen at a given wavelength and may result if the light from the star is not accurately centered on the diode array when observing with the LSA. A second difficulty involves vignetting for SSA data, since the majority of the calibration data was taken with the LSA and the two apertures do not view exactly the same portion of the photocathode at a given wavelength.

The echelle gratings still have difficulties due to the lack of calibration data. Echelle A has a rough sensitivity calibration, but no vignetting or on-orbit blaze function determination. Echelle B is better determined, but still has errors resulting from inadequate sampling. In figure 13 we show the effects of applying the full, multi-dimensional calibration to one of the echelle WSCANS. The dashed line shows the reference spectrum, which has been displaced from the echelle observation for clarity. While there is general overall agreement there are slight discrepancies, many of which probably result from errors in the vignetting function. It is hoped that calibration tests taken after the servicing mission will resolve these difficulties.